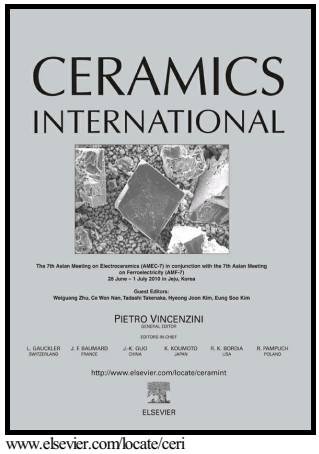


www.elsevier.com/locate/ceri

# Influence of yttrium doping on the structural, morphological and optical properties of nanostructured ZnO thin films grown by spray pyrolysis

O. Bazta, A. Urbieta, J. Piqueras, P. Fernández, M. Addou, J.J. Calvino, A.B. Hungría

PII: S0272-8842(18)33578-8
DOI: https://doi.org/10.1016/j.ceramint.2018.12.178
Reference: CERI20404

To appear in: *Ceramics International*

Received date: 26 October 2018
Revised date: 23 December 2018
Accepted date: 24 December 2018

Cite this article as: O. Bazta, A. Urbieta, J. Piqueras, P. Fernández, M. Addou, J.J. Calvino and A.B. Hungría, Influence of yttrium doping on the structural, morphological and optical properties of nanostructured ZnO thin films grown by spray pyrolysis, *Ceramics International,* https://doi.org/10.1016/j.ceramint.2018.12.178

# Influence of yttrium doping on the structural, morphological and optical properties of nanostructured ZnO thin films grown by spray pyrolysis

**O. Bazta[1,3*], A. Urbieta[2], J. Piqueras[2], P. Fernández[2], M. Addou[3], J.J. Calvino[1], A.B. Hungría[1]**

[1]Department of Materials Science and Metallurgical Engineering and Inorganic Chemistry, University of Cadiz, Cadiz, Spain

[2]Department of Physics, Complutense University of Madrid, Madrid, Spain

[3]Department of Physics, University Abdelmalek Essaadi FST, Tangier, Morocco

*Corresponding author address: otman.bazta@alum.uca.es

**Abstract:**

This study reports on the deposition of highly transparent, n-type ZnO thin films on glass substrate at 450 ºC using spray pyrolysis processing, with the simultaneous insertion of yttrium (Y) at different percentages (0, 2, 5, 7 at.%) as a dopant. The effect of Y doping on the structure, morphology and optical properties of Y doped ZnO (ZnO:Y) was investigated for optoelectronic applications. The obtained thin films were characterized by means of X-ray diffraction, field-emission scanning electron microscopy (FESEM), UV-visible absorbance measurements, photoluminescence (PL) and cathodoluminescence (CL) spectroscopy. The as-prepared films exhibit well-defined hexagonal wurtzite structure grown along [002]. Field emission scanning electron microscope micrographs of the pure ZnO and ZnO:Y showed that the films acquired a dominance of hexagonal-like grains, the morphology was influenced by Y incorporation. All the films showed high transparency in the visible domain with an average transmittance of 83%. The band gap energy, $E_g$, increased from 3.12 eV to 3.18 eV by increasing the Y doping concentration up to 5 at.% and then decreased to 3.15 eV

for 7 at.% Y content. The PL and CL measurements reveal a strong ultraviolet (UV) emission, suggesting that the as-prepared ZnO:Y thin films can potentially be used in optoelectronic devices.

**Keywords:** A. Films; C. Optical properties; D. ZnO; Y doped; Spray pyrolysis

## 1. Introduction

In recent years, transparent conducting oxide (TCO) thin films have attracted attention worldwide due to their envisaged potential application in the domain of optoelectronics, gas sensors and solar cells[1][2][3][4]. Indium tin oxide (ITO) is recognized as the most commonly and widely employed oxide as a TCO material, due to its remarkable features [5], such as high transparency in the visible region, low resistivity and mechanical hardness [6][7] . However, ITO suffers from some drawbacks, for instance a high vacuum deposition process, high cost and deposition temperature, these issues having triggered the search of suitable alternatives [8].

ZnO is considered a promising II-VI semiconductor oxide to replace ITO due to its unique physical and optical properties. Among these, it is particularly outstanding its wide band gap of 3.37eV at room temperature, and the large exciton binding energy of 60 meV; besides that, the n-type conductivity, the high transparency in the visible region and, finally, its excellent chemical and thermal stability are also remarkable properties [9][10][11]. This explains the interest raised in the preparation and nanostructured of ZnO based materials, in forms such as nanowires, thin films, nanotubes or simply as powders made up of nanosized crystallites [12][13] .

Furthermore, the potential and versatility of ZnO based material for a wide range of applications [11], such as solar cells [15][16] gas sensor [14][18], phosphors [19] or as light-emitting diodes (LEDs) [20] have also been demonstrated. For these purposes, the properties of ZnO can be controlled by incorporating aliovalent elements as dopants, such as Al, Li, Sn, Ga or Ni[21,22][23][24][25], in order to improve its structural, optical and electrical features.

Earlier studies have attracted great attention on the use of rare earth (RE) like Eu, Ce or Nd as dopants [26][27], due to their proved capacity to enhance the electrical and optical properties of ZnO. In particular, Y is considered as a suitable ZnO dopant [28][29][30]. In fact, the choice of Y as a dopant is primarily motivated by its close atomic radius to that of Zinc, which facilitates the Y ions insertion into ZnO lattice [31]. Thus, recent studies have demonstrated the capability of Y as a dopant to ameliorate the electrical and optical features of ZnO, as well to decrease its native point defect densities [28][30][32][33]. For instance, Han et al.[28] found that the resistivity of YZO thin films was diminished by adding Y doping at different levels. Li et al.[34] reported that a large number of electrons were introduced after incorporating Y in the lattice of ZnO, and therefore increased the conductivity. In this context, several routes, such as sol-gel [35][36], hydrothermal [37][38], chemical vapor deposition [39] or electrochemical deposition [40] have been tested to develop and enhance the properties of ZnO based materials with various morphologies.

However, to the best of our knowledge, the preparation of Y modified ZnO thin films via spray pyrolysis and the characterization of their optical properties, by combined use of PL and CL, have not been yet considered. Despite the very interesting features which characterize this route, such as its low cost, its large deposition area

capability, allowance of a direct control of film thickness or the use of low temperature growing conditions. Therefore, in this work we explore further this approach to grow ZnO:Y thin films.

In particular, we focus on the optimization of the growth conditions of Y-doped ZnO thin films on glass substrates. The structural characterization of the grown films, by X-ray diffraction (XRD) and scanning electron microscopy (SEM), as well as of key optical properties, such as UV transparency, PL and CL at room temperature, are also investigated.

## 2. Experimental Method

The precursors, zinc chloride ($ZnCl_2$) and yttrium acetate hydrate ($(CH_3CO_2)_3Y$ $xH_2O$) were of analytical grade purchased from Sigma Aldrich and were used without further purification.

The chemical spray pyrolysis procedure used to grow, on glass substrates, both the pure and Y doped ZnO thin films has been reported elsewhere [41]. The investigated Y doping range was 2-7 at.% and growth was performed at 450 ºC. Prior to deposition, the glass substrates were first cleaned in detergent, rinsed in distilled water, acetone and, finally, in distilled water once more. The spraying solution was prepared from a mixture of 0.05 M Zinc chloride, as a source of zinc oxide, and yttrium acetate hydrate, as dopant source, in different concentrations (2,5,7at.%). A small amount of hydrochloric acid (HCl) was added to this solution in order to prevent the formation of zinc hydroxide ($Zn(OH)_2$). The substrates were placed onto a hotplate and preheated to 450 ºC. The nozzle was kept at a distance of 40 cm from the substrate during the deposition. Compressed air was employed as a carrier gas with a spray rate of 2 ml/min during 6

min. Regular pauses to the deposition were taken into account to allow the substrate to return to the set temperature. The optimum conditions determined to prepare the ZnO:Y thin films are displayed in Table 1.

X-ray diffraction (XRD) diagrams of the prepared films were recorded by X-ray diffraction (Bruker D8 advance X-ray diffractometer). Surface morphology for coated films was investigated via scanning electron microscopy (SEM, Nova NanoSEM 450). Average crystallite size were determined both, by the Scherrer method from the broadening of the diffraction peaks, and from FESEM images. The optical transmission spectra were recorded on a Shimadzu UV-1603 UV-Visible spectrophotometer. The room temperature photoluminescence (PL) spectra were recorded using a confocal Horiba Jobin Yvon Labram HR 800 with excitation wavelength 325 nm. Cathodoluminescence spectra were collected in a Leica 440 SEM equipped with a CCD Hamamatsu PMA-11.



**3. Results and discussion**

XRD analysis was carried out to investigate the effect of Y doping on crystal structure and phase changes of the ZnO host matrix. Figure 1a displays the diffractograms of the different ZnO thin films prepared by the chemical spray pyrolysis technique. In all samples, the diffractograms show the same peaks indicating that the crystal structure of the specimens is hexagonal (wurtzite) with highly preferential orientation along [002], in good agreement with previous results reported by Lim, J. H. et al.,[42] and Maller et al [43] for Al, Ga and In-doped ZnO. No additional peaks due to segregated Y-rich phases were found in any of the investigated films, indicating a

high phase homogeneity and hence, a good incorporation of $Y^{3+}$ ions into the host ZnO matrix.

The intensity of the (002) peak is maximum for ZnO:Y 5 at.% films, showing that the films have a crystalline nature even after doping. A decrease in the intensity of (002) reflection is noticed after increasing the doping concentration beyond 5 at.%, which suggests a loss of crystallinity, very likely due to the segregation of Y at grain boundaries for high doping contents. Fig. 1b illustrates the shifting of the (002) peak position with Y concentration. Over the doping range investigated, it can be observed that in ZnO: Y films the position of the (002) peak shifts gradually to the lower scattering angle (2θ) side while increasing doping concentration up to ZnO: Y 5 at.%. This trend may be attributed to a substitution of $Zn^{2+}$ (0.74 Å) by $Y^{3+}$ ions (0.92 Å), which may also generate some lattice strain. In contrast, doping at a concentration of 7% at. results in a decrease in the (002) peak shift. The interplanar spacing $d_{hkl}$ values of ZnO:Y thin films were calculated by using the Bragg equation [44]:

$$2d_{hkl} \sin\theta = n\lambda \qquad (1)$$

The lattice parameters for all the films were estimated from (002) and (100) d-values, according to the following equation [45]:

$$\left(\frac{1}{d_{hkl}}\right)^2 = \frac{4}{3}\left(\frac{h^2+k^2+hk}{a^2}\right) + \left(\frac{l^2}{c^2}\right) \qquad (2)$$

The interplanar and lattice parameters are summarized in Table 2a. Results reveal a slight increase in the lattice parameters after Y-doping up to 2 at.%.

The crystallite size of pure and Y doped ZnO was determined based on the broadening of the preferential orientation (002) using the Debye-Scherrer's formula [46]:

$$D = \frac{k\lambda}{\beta \cos\theta} \qquad (3)$$

Where k represents the shape factor, β is the full width at half maximum in radian of (002) orientation, $\lambda$ is the X-ray wavelength and $\theta$ is the Bragg's angle of the X-ray diffraction peak. The values of crystallite size for the different samples, listed in Table 2.b, fall in the range between 48 and 52 nm. It increases with doping up to 5 at.%. however, decreases at 7 at.%.

Microstrain $\varepsilon$ for each film was also determined by using the tangent formula[47]:

$$\varepsilon = \frac{\beta}{4tan\theta} \qquad (4)$$

Noticeable, micro strain for the (002) plane decreases with increasing doping concentration from 0% to 5 at.%, which may be due to the release of stress in the films, which indicates that doping by Y improves the crystallization of the films. In addition, the ZnO:Y 5 at.% gives the minimum of structural defects.

This structural study points out that the incorporation of Y improves the structural quality of sprayed ZnO thin films, by increasing the crystallite size (D) while decreasing the micro-strain. Nevertheless, a 5 at.% doping limit is detected to observe this effect. This phenomenon is consistent with the influence of Y doping on the structural parameters observed for the thin films. XRD analysis also shows that Y ions were successfully introduced into ZnO lattice without generating any secondary phase.

Representative FE-SEM micrographs (magnification 30000) of ZnO:Y films are shown in Fig. 2a-b ((a) 0 at.% Y, (b) 7 at.% Y). At room temperature, the FE-SEM micrographs demonstrate the predominance of hexagonal-shaped ZnO crystals. FE-SEM micrographs reveal that the size of the crystallites assembled into the synthesized

films falls within the nanometer range size. Absence of cracks is observed on large areas of all films. The ZnO film image reveals a very homogeneous distribution of connected nanoparticles over the surface, mostly hexagonal in shape, but with a small fraction of spheroid or rod-like ones. The film grown with a [Y]/ [Zn] ratio=0.05 exhibits a dense surface structure composed of crystallites in the hexagonal form, in good agreement with the X-ray diffraction results. On the other hand, it is evident that the porous structure and visibly lower homogeneity in morphology occurred throughout the film formulated with 7 at.% of Y.

Based on FESEM images, the particle size distribution of all the samples was estimated considering 200 individual particles, Table 2.b and Fig.2e. Close values are observed for the intermediate doping levels, whereas lower particle sizes are measured for the undoped and 7 at.% at Y samples. Two factors can contribute to this difference. First SEM measures particle size, whereas XRD provides values of crystallite size. Since XRD data correspond to volume averaged values and SEM data to a linear average, the difference found in this case suggests that in all the samples, particularly in the 2 at.% and 5 at.% Y, particles consist of crystalline aggregates, i.e. particles are not monocrystalline. Another question that could contribute to this difference could be the eventual anisotropy in particle shape, since measurements in the SEM images are performed in a direction parallel to the film surface and XRD provides a size which takes into account different directions. These differences have been also found in Al-doped ZnO films prepared by spray pyrolysis [48].

On the other hand, the chemical composition of ZnO:Y films was confirmed by energy dispersive X-ray spectroscopy (XEDS). The XEDS spectra, Figure 3, reveal the

presence of the expected elements Y, Zn and O in the solid films. Quantification of these spectra indicates percentages of Y close to the nominal values.

Regarding optical properties, both absorbance and transmittance spectra in the UV-VIS range have been measured. Fig. 4 shows the transmittance (a) and absorption (b) spectra of the different films in the wavelength range 300-1000 nm, respectively. The transmittance spectra, Figure 4a, reveal a very high transmittance over the visible domain, between 80% and 83%, confirming the high transparency of all the synthesized films and the low scattering impacts related to the homogeneity and smoothness of the films without and with presence of Y as evidenced from the XRD and SEM studies. Remarkably, this result is comparatively higher than those previously published where the transmission was found in range 70-82% [49][50]. The transmission is maximal for pure ZnO film and it slightly decreases with incorporation of the Y. This reduction is likely to be interpreted in terms of variations of film thicknesses. These results are in good agreement with those of Salah et al. on ZnO films modified with different dopants [51]. In addition to the main band, the transmission spectra of the investigated films exhibit some shoulders, which can be attributed to the existence of defects and porosity inside the films [52]. The optical band gap of pure and Y modified ZnO films was estimated from the absorption spectra based on a model suggested by Tauc, and using the following equation which correlates the optical band gap and the absorption coefficient[53]:

$$(\alpha h\nu)^2 = A\left(h\nu - E_g\right) \qquad (5)$$

In which A is a constant, hυ is the photon energy, $E_g$ represents the optical band gap and α is the absorption coefficient.

Fig.5 shows the plots of $(\alpha h\upsilon)^2 = f(h\upsilon - E_g)$ for pure and ZnO:Y thin films. The optical band gap value can be determined by extrapolation of the straight line at $\alpha = 0$. The obtained values of optical band gap energy of ZnO:Y as a function of Y concentration are reported in table 3.

To confirm the reported optical band gap energy values via Tauc's plot, the first derivative of the transmittance (dT/dE) method has been also used [54]. Fig.6 shows the plot of dT/dE versus energy ($h\upsilon$) where it can be seen that the optical band gap $E_g$ values using the derivative of the transmittance are equal to those obtained by means of Tauc's method.

The band gap energy $E_g$ value was found to increase from 3.12 eV to 3.18 eV by increasing the doping content up to 0.05 at.%, followed by a decrease for higher Y level. This shift towards higher energies could be explained by the differences in the lattice parameters or the increase of the carrier concentration (Burstein–Moss effect) [55][56].The shift towards lower energies for the higher doping levels could be attributed to the apparition of energy states in the forbidden band close to the band edges This phenomenon is described by Urbach´s empirical law, which can be expressed using the following relation [57];

$$\alpha = \alpha_0 \exp\left(\frac{h\upsilon}{E_u}\right) \qquad (6)$$

$$\text{i.e. } E_u = \left[\frac{d\ln\alpha}{dh\upsilon}\right]^{-1}$$

Where $\alpha_0$ is a constant, $\alpha$ represents the experimentally optical absorption and $E_u$ corresponds to the width of the Urbach tail.

The numerical value of $E_u$ is deduced from the reverse of the slope of the Fig.7. The obtained values are summarized in table 4. $E_u$ value was found to change inversely with optical band gap. Fig.8 illustrates the variation of Urbach energy together with optical band gap as a function of Y doping level. We note that a decrease of the Urbach energy by increasing the Y doping up to 5 at.%, which implied that the incorporation of Y at low concentrations (from 0 up to 5 at.%) led to a decrease in structural disorders and defects in agreement with XRD analysis data that reveals an increase in degree of crystallinity of the films.

The luminescence properties of ZnO have been widely studied; however, still many points remain unclear. In the present work, both photo- and cathodoluminescence measurements have been performed.

Room temperature PL spectra of the ZnO:Y thin films, excited with 325 nm wavelength, are shown in Fig. 9. PL spectra show that all the films exhibit an intense UV emission peak, corresponding to the near band edge emission [58]. A broad band associated to defects are also visible in the undoped and the less doped samples [59]. Deep level band extends from green to red region, the most intense components are located around 580 nm and 650 nm, however a shoulder in the green region is also observed (figure 9a). Deep level band may be fitted to the experimental data by deconvolution of the spectra in two Lorentzian peaks, located at 596 nm (named as $P_1$) and 660 nm (named $P_2$). The first component (yellow and orange emission), observed solely in undoped and 2 at.% Y doped ZnO films, is sometimes ascribed to the oxygen vacancies or impurities [60][61]. The shoulder in the green region is a typical band for ZnO and disappeared after Y doping incorporation [62]. The red component, named as

$P_2$ corresponds to a transition between ionized and neutral oxygen atoms, normally associated to excess of oxygen [63][64]. By comparing the PL spectra of undoped and Y-doped films, it seems clear that the incorporation of Y suppresses the deep level defects and reinforces the UV emission. It is worthy to note that the most commonly reported band for this material, the green band, is almost absent in these samples. Oxygen vacancies are usually reported to be responsible for this band [65], hence the low emission in the green region and the higher intensity of the red component would both point to the oxygen excess mentioned above. Figures 9b-d show the spectra obtained from doped samples, the main difference with respect to the undoped samples, is the progressive decrease of the deep level band. Table 5 shows the ratios of the NBE to the DL emission for the different dopant contents. This ratio increases from 2.82 in the undoped sample to 20.71 in the most heavily doped, where the DL band is practically absent (figure 9d). Besides the decrease in the relative intensity of the deep level band, the NBE, a slight shift towards lower wavelength can be observed. Both effects are illustrated in the graphs of figures 10 and 11. The shift with the Y content is consistent with values obtained for the optical band gap found from Tauc´s model. It is also observed that the NBE intensity depends markedly on the Y concentration and increases considerably with the doping content (2 , 5 and 7 at.%). For instance, when the Y concentration increases to 7 at%, the intensity of the UV emission is about 5 times higher than that of the pure ZnO. Therefore, the incorporation of Y into the ZnO matrix decreases the non-radiative recombination process resulting in a higher relative intensity in the Y doped films. The $I_{uv}/I_{vis}$ ratio could be taken as an indication of the quality of the sample, since the visible emission is related to defects. The increase of the relative

intensity of the NBE emission would point to a decrease of the defect concentration as the dopant content increases, in agreement with the XRD results.

CL measurements were carried out to get a further, complementary, insight about the quality and purity of the material. This technique can also provide valuable information regarding the distribution of defects and impurities into the ZnO matrix. The emission bands observed in photo- and cathodoluminescence should be essentially the same; however, the different excitation conditions may be responsible for different relative intensity ratios between the different components. Thus gives the possibility to observe additional features. As has been already mentioned for PL, two main emissions are usually observed in the CL spectra of ZnO, the near band edge emission in the UV range, and the green band. Besides those, an orange-red band is frequently observed and ascribed to several impurities [66][67]. Typical CL spectra are shown in Fig.12. The deconvoluted CL spectra show that all the films exhibit the three main bands already referred; a sharp UV emission, a green emission and a red emission. The sharp UV emission, which is close to the optical band gap transition of undoped and Y-doped ZnO estimated above, is related to the band to band emission. Moreover, the UV emission intensity depends strongly on the Y doping concentration, and increases with increasing Y content up to 5at.%. At this concentration, a maximum is observed. Additionally, the presence of an intense band-edge emission indicates a good quality and crystallinity of the films. The green emission points out to the presence of defects in the crystal structure, such as O-vacancies (Vo) or O-interstitial (Oi) [68]. The weaker emission observed from about 640 to 650 nm corresponds to the orange-red band observed in PL.

Finally, Fig.13 depicts the evolution of $I_{UV}/I_{DLE}$ ratio as a function of Y doping concentration. It can be noticed that the as-deposited ZnO:Y thin films exhibit a very high intensity ratio of UV emission over the green emission, which indicates that the ZnO:Y films are highly crystalline with scarce oxygen deficiencies. These findings reveal that the Y-doped ZnO films can exhibit a high crystallization state that is very likely promoted by Y doping. Moreover, the whole set of optical response characterization data prove that the films prepared in the present work can be utilized in optoelectronic applications, mostly due to their remarkably strong UV emission.

## 4. Conclusions

In summary, pure and Y-doped ZnO were successfully deposited on a glass-preheated substrate at 450 ºC by a facile spray pyrolysis method. The influence of incorporation of Y on structural, morphological and optical properties of ZnO crystal lattice was investigated. XRD spectra reveal that all sprayed films are polycrystalline with a hexagonal wurtzite structure and strongly oriented towards the [002] direction. SEM micrographs illustrate that all the films exhibit a dense surface structure with a hexagonal shape grains. The calculated structural parameters evidence that the incorporation of Y entails a decrease in the microstrain, which demonstrates that doping with $Y^{3+}$ ions actually improve the quality of the as-deposited films. The UV-visible study shows that all the films are highly transparent in the visible domain. The results obtained by PL and CL of sprayed ZnO:Y thin films reveal that the incorporation of Y markedly improves the UV emission intensity while, at the same time, suppresses the deep level emission of ZnO and increases the UV/DLE intensity ratio. This improved

UV emission performance confirms that ZnO:Y system offer potential applications in optoelectronic devices.

**Acknowledgment**

This work was supported by MINECO/FEDER (MAT 2016-81118-P and MAT 2015-65274-R). O. B. thanks Aula del Estrecho fellowship.

**References**

[1] A.P. Chatterjee, P. Mitra, A.K. Mukhopadhyay, Chemically deposited zinc oxide thin film gas sensor, J. Mater. Sci. 34 (1999) 4225–4231. doi:10.1023/A:1004694501646.

[2] T. Minami, T. Miyata, K. Ihara, Y. Minamino, S. Tsukada, Effect of ZnO film deposition methods on the photovoltaic properties of ZnO-Cu2O heterojunction devices, Thin Solid Films. 494 (2006) 47–52. doi:10.1016/j.tsf.2005.07.167.

[3] E. Fazio, A.M. Mezzasalma, G. Mondio, T. Serafino, F. Barreca, F. Caridi, Optical and structural properties of pulsed laser ablation deposited ZnO thin film, Appl. Surf. Sci. 257 (2011) 2298–2302. doi:10.1016/j.apsusc.2010.09.092.

[4] F. Gao, X.Y. Liu, L.Y. Zheng, M.X. Li, Y.M. Bai, J. Xie, Microstructure and optical properties of Fe-doped ZnO thin films prepared by DC magnetron sputtering, J. Cryst. Growth. 371 (2013) 126–129. doi:10.1016/j.jcrysgro.2013.02.027.

[5] A. Mohammadi Gheidari, E. Asl Soleimani, M. Mansorhoseini, S. Mohajerzadeh, N. Madani, W. Shams-Kolahi, Structural properties of indium tin

oxide thin films prepared for application in solar cells, Mater. Res. Bull. 40 (2005) 1303–1307. doi:10.1016/j.materresbull.2005.04.007.

[6] A. El Hichou, A. Kachouane, J.L. Bubendorff, M. Addou, J. Ebothe, M. Troyon, A. Bougrine, Effect of substrate temperature on electrical, structural, optical and cathodoluminescent properties of In2O3-Sn thin films prepared by spray pyrolysis, Thin Solid Films. 458 (2004) 263–268. doi:10.1016/j.tsf.2003.12.067.

[7] A.M. Bazargan, F. Sharif, S. Mazinani, N. Naderi, A high quality ITO/PET electrode for flexible and transparent optoelectronic devices, J. Mater. Sci. Mater. Electron. 28 (2017) 2962–2969. doi:10.1007/s10854-016-5881-7.

[8] W. He, C. Ye, Flexible Transparent Conductive Films on the Basis of Ag Nanowires: Design and Applications: A Review, J. Mater. Sci. Technol. 31 (2015) 581–588. doi:10.1016/j.jmst.2014.11.020.

[9] S. Aksoy, Y. Caglar, S. Ilican, M. Caglar, Sol-gel derived Li-Mg co-doped ZnO films: Preparation and characterization via XRD, XPS, FESEM, J. Alloys Compd. 512 (2012) 171–178. doi:10.1016/j.jallcom.2011.09.058.

[10] V. Kumar, V. Kumar, S. Som, A. Yousif, N. Singh, O.M. Ntwaeaborwa, A. Kapoor, H.C. Swart, Effect of annealing on the structural, morphological and photoluminescence properties of ZnO thin films prepared by spin coating, J. Colloid Interface Sci. 428 (2014) 8–15. doi:10.1016/j.jcis.2014.04.035.

[11] N.A. Hammed, A.A. Aziz, A.I. Usman, M.A. Qaeed, The sonochemical synthesis of vertically aligned ZnO nanorods and their UV photodetection properties: Effect of ZnO buffer layer, Ultrason. Sonochem. 50 (2018) 172–181. doi:10.1016/j.ultsonch.2018.09.020.

[12] M.A. Zimmler, F. Capasso, S. Müller, C. Ronning, Optically pumped nanowire

lasers: Invited review, Semicond. Sci. Technol. 25 (2010). doi:10.1088/0268-1242/25/2/024001.

[13] L. Zhu, Y. Li, W. Zeng, Hydrothermal synthesis of hierarchical flower-like ZnO nanostructure and its enhanced ethanol gas-sensing properties, Appl. Surf. Sci. 427 (2018) 281–287. doi:10.1016/j.apsusc.2017.08.229.

[14] Z. Hou, Y. Wang, L. Shen, H. Guo, G. Wang, Y. Li, S. Zhou, Synthesis of dumbbell-like ZnO microcrystals via a simple solution route, (2012) 1–7.

[15] N. Jabena Begum, K. Ravichandran, Effect of source material on the transparent conducting properties of sprayed ZnO:Al thin films for solar cell applications, J. Phys. Chem. Solids. 74 (2013) 841–848. doi:10.1016/j.jpcs.2013.01.029.

[16] X. Ren, W. Zi, Q. Ma, F. Xiao, F. Gao, S. Hu, Y. Zhou, S. Liu, Topology and texture controlled ZnO thin film electrodeposition for superior solar cell efficiency, Sol. Energy Mater. Sol. Cells. 134 (2015) 54–59. doi:10.1016/j.solmat.2014.11.026.

[17] A.P. Rambu, L. Ursu, N. Iftimie, V. Nica, M. Dobromir, F. Iacomi, Study on Ni-doped ZnO films as gas sensors, Appl. Surf. Sci. 280 (2013) 598–604. doi:10.1016/j.apsusc.2013.05.033.

[18] M. Yin, S. Liu, One-pot synthesis of Co-doped ZnO hierarchical aggregate and its high gas sensor performance, Mater. Chem. Phys. 149 (2015) 344–349. doi:10.1016/j.matchemphys.2014.10.027.

[19] M. Willander, O. Nur, J.R. Sadaf, M.I. Qadir, S. Zaman, A. Zainelabdin, N. Bano, I. Hussain, Luminescence from zinc oxide nanostructures and polymers and their hybrid devices, Materials (Basel). 3 (2010) 2643–2667. doi:10.3390/ma3042643.

[20] N. Srinatha, P. Raghu, H.M. Mahesh, B. Angadi, Spin-coated Al-doped ZnO thin films for optical applications: Structural, micro-structural, optical and luminescence studies, J. Alloys Compd. 722 (2017) 888–895. doi:10.1016/j.jallcom.2017.06.182.

[21] B. V. Shrisha, S. Bhat, D. Kushavah, K. Gopalakrishna Naik, Hydrothermal growth and characterization of Al-doped ZnO nanorods, Mater. Today Proc. 3 (2016) 1693–1701. doi:10.1016/j.matpr.2016.04.061.

[22] N. Chahmat, T. Souier, A. Mokri, M. Bououdina, M.S. Aida, M. Ghers, Structure, microstructure and optical properties of Sn-doped ZnO thin films, J. Alloys Compd. 593 (2014) 148–153. doi:10.1016/j.jallcom.2014.01.024.

[23] R.H. Horng, S.L. Ou, C.Y. Huang, P. Ravadgar, C.I. Wu, Effects of Ga concentration and rapid thermal annealing on the structural, optoelectronic and photoluminescence properties of Ga-doped ZnO thin films, Thin Solid Films. 605 (2016) 30–36. doi:10.1016/j.tsf.2015.12.006.

[24] D. İskenderoğlu, H. Güney, Synthesis and characterization of ZnO:Ni thin films grown by spray-deposition, Ceram. Int. 43 (2017) 16593–16599. doi:10.1016/j.ceramint.2017.09.047.

[25] Y. Ortega, P. Fernández, J. Piqueras, Growth and luminescence of oriented nanoplate arrays in tin doped ZnO, Nanotechnology. 18 (2007). doi:10.1088/0957-4484/18/11/115606.

[26] J.C. Sin, S.M. Lam, K.T. Lee, A.R. Mohamed, Preparation of rare earth-doped ZnO hierarchical micro/nanospheres and their enhanced photocatalytic activity under visible light irradiation, Ceram. Int. 40 (2014) 5431–5440. doi:10.1016/j.ceramint.2013.10.128.

[27] J. Jiang, K. Zhang, X. Chen, F. Zhao, T. Xie, D. Wang, Y. Lin, Porous Ce-doped ZnO hollow sphere with enhanced photodegradation activity for artificial waste water, J. Alloys Compd. 699 (2017) 907–913. doi:10.1016/j.jallcom.2017.01.036.

[28] X. Han, K. Han, M. Tao, Low Resistivity Yttrium-Doped Zinc Oxide by Electrochemical Deposition, J. Electrochem. Soc. 157 (2010) H593. doi:10.1149/1.3377092.

[29] J. Yang, R. Wang, L. Yang, J. Lang, M. Wei, M. Gao, X. Liu, J. Cao, X. Li, N. Yang, Tunable deep-level emission in ZnO nanoparticles via yttrium doping, J. Alloys Compd. 509 (2011) 3606–3612. doi:10.1016/j.jallcom.2010.12.102.

[30] P.-T. Hsieh, R.W.-K. Chuang, C.-Q. Chang, C.-M. Wang, S.-J. Chang, Optical and structural characteristics of yttrium doped ZnO films using sol–gel technology, J. Sol-Gel Sci. Technol. 58 (2011) 42–47. doi:10.1007/s10971-010-2352-0.

[31] M. Gao, J. Yang, L. Yang, Y. Zhang, J. Lang, H. Liu, H. Fan, Y. Sun, Z. Zhang, H. Song, Enhancement of optical properties and donor-related emissions in Y-doped ZnO, Superlattices Microstruct. 52 (2012) 84–91. doi:10.1016/j.spmi.2012.03.016.

[32] R. Kaur, A. V. Singh, R.M. Mehra, Structural, electrical and optical properties of sol-gel derived yttrium doped ZnO films, Phys. Status Solidi. 202 (2005) 1053–1059. doi:10.1002/pssa.200420006.

[33] L. li Yang, J. hai Yang, D. dan Wang, Y. jun Zhang, Y. xin Wang, H. lian Liu, H. gang Fan, J. hui Lang, Photoluminescence and Raman analysis of ZnO nanowires deposited on Si(1 0 0) via vapor-liquid-solid process, Phys. E Low-Dimensional

Syst. Nanostructures. 40 (2008) 920–923. doi:10.1016/j.physe.2007.11.025.

[34] X.B. Li, Q.Q. Zhang, S.Y. Ma, G.X. Wan, F.M. Li, X.L. Xu, Microstructure optimization and gas sensing improvement of ZnO spherical structure through yttrium doping, Sensors Actuators, B Chem. 195 (2014) 526–533. doi:10.1016/j.snb.2014.01.087.

[35] T. Ivanova, A. Harizanova, T. Koutzarova, B. Vertruyen, Sol-gel derived ZnO:Y nanostructured films: Structural and optical study, Colloids Surfaces A Physicochem. Eng. Asp. 532 (2017) 363–368. doi:10.1016/j.colsurfa.2017.04.065.

[36] G. Turgut, S. Duman, E.F. Keskenler, The influence of Y contribution on crystallographic, topographic and optical properties of ZnO: A heterojunction diode application, Superlattices Microstruct. 86 (2015) 363–371. doi:10.1016/j.spmi.2015.08.002.

[37] Y. He, T. Yanagida, K. Nagashima, F. Zhuge, G. Meng, B. Xu, A. Klamchuen, S. Rahong, M. Kanai, X. Li, M. Suzuki, S. Kai, T. Kawai, Crystal-plane dependence of critical concentration for nucleation on hydrothermal ZnO nanowires, J. Phys. Chem. C. 117 (2013) 1197–1203. doi:10.1021/jp3113232.

[38] L. Schlur, A. Carton, P. Lévêque, D. Guillon, G. Pourroy, Optimization of a New ZnO Nanorods Hydrothermal Synthesis Method for Solid State Dye Sensitized Solar Cells Applications, J. Phys. Chem. C. 117 (2013) 2993–3001. doi:10.1021/jp305787r.

[39] S.W. Kim, S. Fujita, H.K. Park, B. Yang, H.K. Kim, D.H. Yoon, Growth of ZnO nanostructures in a chemical vapor deposition process, J. Cryst. Growth. 292 (2006) 306–310. doi:10.1016/j.jcrysgro.2006.04.026.

[40] X. Ren, W. Dang, Q. Ma, X. Zhu, W. Zi, L. Jia, B. Liu, X. Zhang, F. Xiao, H. Yang, Z. Yang, S.F. Liu, Superior texture-controlled ZnO thin film using electrochemical deposition, Sol. Energy. 125 (2016) 192–197. doi:10.1016/j.solener.2015.12.018.

[41] M. El Jouad, M. Alaoui Lamrani, Z. Sofiani, M. Addou, T. El Habbani, N. Fellahi, K. Bahedi, L. Dghoughi, A. Monteil, B. Sahraoui, S. Dabos, N. Gaumer, Roughness effect on photoluminescence of cerium doped zinc oxide thin films, Opt. Mater. (Amst). 31 (2009) 1357–1361. doi:10.1016/j.optmat.2008.10.031.

[42] J.H. Lim, S.M. Lee, H.-S. Kim, H.Y. Kim, J. Park, S.-B. Jung, G.C. Park, J. Kim, J. Joo, Synergistic effect of Indium and Gallium co-doping on growth behavior and physical properties of hydrothermally grown ZnO nanorods, Sci. Rep. 7 (2017) 41992. doi:10.1038/srep41992.

[43] R. Maller, Y. Porte, H.N. Alshareef, M.A. McLachlan, Probing the doping mechanisms and electrical properties of Al, Ga and In doped ZnO prepared by spray pyrolysis, J. Mater. Chem. C. 4 (2016) 5953–5961. doi:10.1039/C5TC03636D.

[44] O. Lupan, T. Pauporté, L. Chow, B. Viana, F. Pellé, L.K. Ono, B. Roldan Cuenya, H. Heinrich, Effects of annealing on properties of ZnO thin films prepared by electrochemical deposition in chloride medium, Appl. Surf. Sci. 256 (2010) 1895–1907. doi:10.1016/j.apsusc.2009.10.032.

[45] N. El-Kadry, A. Ashour, S.A. Mahmoud, Structural dependence of d.c. electrical properties of physically deposited CdTe thin films, Thin Solid Films. 269 (1995) 112–116. doi:10.1016/0040-6090(95)06869-4.

[46] S.J.S. Qazi, A.R. Rennie, J.K. Cockcroft, M. Vickers, Use of wide-angle X-ray

diffraction to measure shape and size of dispersed colloidal particles, J. Colloid Interface Sci. 338 (2009) 105–110. doi:10.1016/j.jcis.2009.06.006.

[47] P.P. Sahay, R.K. Nath, Al-doped ZnO thin films as methanol sensors, Sensors Actuators, B Chem. 134 (2008) 654–659. doi:10.1016/j.snb.2008.06.006.

[48] L. Dghoughi, F. Ouachtari, M. Addou, B. Elidrissi, H. Erguig, A. Rmili, A. Bouaoud, The effect of Al-doping on the structural, optical, electrical and cathodoluminescence properties of ZnO thin films prepared by spray pyrolysis, Phys. B Condens. Matter. 405 (2010) 2277–2282. doi:10.1016/j.physb.2010.02.025.

[49] R. Mariappan, V. Ponnuswamy, A. Chandra Bose, R. Suresh, M. Ragavendar, Influence of y doping concentration on the properties of nanostructured MxZn1-xO (M=Y) thin film deposited by nebulizer spray pyrolysis technique, J. Phys. Chem. Solids. 75 (2014) 1033–1040. doi:10.1016/j.jpcs.2014.03.014.

[50] H. Woo Choi, K.S. Lee, N. David Theodore, T.L. Alford, Improved performance of ZnO nanostructured bulk heterojunction organic solar cells with nanowire-density modified by yttrium chloride introduction into solution, Sol. Energy Mater. Sol. Cells. 117 (2013) 273–278. doi:10.1016/j.solmat.2013.06.036.

[51] M. Salah, S. Azizi, A. Boukhachem, C. Khaldi, M. Amlouk, J. Lamloumi, Structural, morphological, optical and photodetector properties of sprayed Li-doped ZnO thin films, J. Mater. Sci. 52 (2017) 10439–10454. doi:10.1007/s10853-017-1218-z.

[52] R. Mimouni, O. Kamoun, A. Yumak, A. Mhamdi, K. Boubaker, P. Petkova, M. Amlouk, Effect of Mn content on structural, optical, opto-thermal and electrical properties of ZnO:Mn sprayed thin films compounds, J. Alloys Compd. 645

(2015) 100–111. doi:10.1016/j.jallcom.2015.05.012.

[53] Q. Yu, H. Yang, W. Fu, L. Chang, J. Xu, C. Yu, R. Wei, K. Du, H. Zhu, M. Li, G. Zou, Transparent conducting yttrium-doped ZnO thin films deposited by sol-gel method, Thin Solid Films. 515 (2007) 3840–3843. doi:10.1016/j.tsf.2006.10.077.

[54] M. Wang, E.J. Kim, S. Kim, J.S. Chung, I.K. Yoo, E.W. Shin, S.H. Hahn, C. Park, Optical and structural properties of sol-gel prepared MgZnO alloy thin films, Thin Solid Films. 516 (2008) 1124–1129. doi:10.1016/j.tsf.2007.05.039.

[55] D. Gherouel, I. Gaied, K. Boubaker, N. Yacoubi, M. Amlouk, Some physical investigations of AgInS2-xSexthin film compounds obtained from AgInS2annealed in seleneide atmosphere, J. Alloys Compd. 545 (2012) 190–199. doi:10.1016/j.jallcom.2012.07.148.

[56] Y.M. Hao, S.Y. Lou, S.M. Zhou, R.J. Yuan, G.Y. Zhu, N. Li, Structural, optical, and magnetic studies of manganese-doped zinc oxide hierarchical microspheres by self-assembly of nanoparticles, Nanoscale Res. Lett. 7 (2012) 1–13. doi:10.1186/1556-276X-7-100.

[57] B. Pejova, The Urbach-Martienssen absorption tails in the optical spectra of semiconducting variable-sized zinc selenide and cadmium selenide quantum dots in thin film form, Mater. Chem. Phys. 119 (2010) 367–376. doi:10.1016/j.matchemphys.2009.08.064.

[58] C. Han, L. Duan, X. Zhao, Z. Hu, Y. Niu, W. Geng, Effect of Fe doping on structural and optical properties of ZnO films and nanorods, J. Alloys Compd. 770 (2019) 854–863. doi:10.1016/j.jallcom.2018.08.217.

[59] T. Jia, W. Wang, F. Long, Z. Fu, H. Wang, Q. Zhang, Synthesis, characterization

and luminescence properties of Y-doped and Tb-doped ZnO nanocrystals, Mater. Sci. Eng. B Solid-State Mater. Adv. Technol. 162 (2009) 179–184. doi:10.1016/j.mseb.2009.04.004.

[60] M.S. Kim, K.G. Yim, D.Y. Kim, S. Kim, G. Nam, D.Y. Lee, S.O. Kim, J.S. Kim, J.S. Kim, J.S. Son, J.Y. Leem, Growth and characterization of seed layer-free ZnO thin films deposited on porous silicon by hydrothermal method, Electron. Mater. Lett. 8 (2012) 75–80. doi:10.1007/s13391-011-0130-y.

[61] K. Vanheusden, C.H. Seager, W.L. Warren, D.R. Tallant, J.A. Voigt, Correlation between photoluminescence and oxygen vacancies in ZnO phosphors, Appl. Phys. Lett. 403 (1995) 403. doi:10.1063/1.116699.

[62] H.-J. Egelhaaf, D. Oelkrug, Luminescence and nonradiative deactivation of excited states involving oxygen defect centers in polycrystalline ZnO, J. Cryst. Growth. 161 (1996) 190–194.

[63] B. Panigrahy, M. Aslam, D.S. Misra, M. Ghosh, D. Bahadur, Defect-related emissions and magnetization properties of ZnO Nanorods, Adv. Funct. Mater. 20 (2010) 1161–1165. doi:10.1002/adfm.200902018.

[64] K. Nadarajah, C. Yern Chee, C.Y. Tan, Influence of annealing on properties of spray deposited ZnO thin films, J. Nanomater. 2013 (2013). doi:10.1155/2013/146382.

[65] J.H. Hong, Y.F. Wang, G. He, J.X. Wang, Tuning visible emission by choosing excitation wavelength in Mg-doped ZnO/silica composites, J. Alloys Compd. 506 (2010) 1–3. doi:10.1016/j.jallcom.2010.06.088.

[66] W. Yan, J. Tan, W. Zhang, Y. Liang, S. Feng, X. Lei, H. Wang, Spray pyrolysis derived ZnMgO:In thin films: Investigation of the structural, optical and

electrical properties, Superlattices Microstruct. 60 (2013) 407–413. doi:10.1016/j.spmi.2013.05.021.

[67] A. El Hichou, M. Addou, A. Bougrine, R. Dounia, J. Ebothé, M. Troyon, M. Amrani, Cathodoluminescence properties of undoped and Al-doped ZnO thin films deposited on glass substrate by spray pyrolysis, Mater. Chem. Phys. 83 (2004) 43–47. doi:10.1016/j.matchemphys.2003.08.015.

[68] S.C. Lyu, Y. Zhang, H. Ruh, H.-J. Lee, H.-W. Shim, E.-K. Suh, C.J. Lee, Low temperature growth and photoluminescence of well-aligned zinc oxide nanowires, Chem. Phys. Lett. 363 (2002) 134–138. doi:10.1016/S0009-2614(02)01145-4.

**Fig. 1** a**)** XRD pattern of ZnO:Y thin films.b) Zoom of (002) peak to show the shift of the peak position as a function of Y content.
**Fig. 2.** SEM images of Y doped ZnO thin films: (a) 0 at.% Y, (b) 2 at.% Y, (c) 5 at.% Y, (d) 7 at.% Y. (e) Crystallite size of undoped and ZnO:Y films as determined from FESEM micrographs and XRD. The lines are eye-guides.
**Fig. 3** Energy dispersive X-ray spectra of Y-doped ZnO films.
**Fig. 4.** (a) Spectral transmission characteristics of pure and ZnO:Y thin films. (b)UV-vis absorption of pure and ZnO:Y thin films.
**Fig.5.** $(\alpha h\nu)^2$ versus $h\nu$ plots of undoped and ZnO: Y sprayed films.
**Fig.6.** Plots of derivative of the transmittance with respect to the photon energy of Y-doped ZnO films
**Fig.7.** The Urbach plots of Y-doped ZnO thin films.
**Fig.8.** Variation of Urbach energy and optical band gap respecting Y content.
**Fig.9.** PL spectra of pure and Y-doped ZnO thin films.
**Fig.10.** Shifting of UV emission with Y content.
**Fig.11.** Evolution of $I_{UV}/I_{DLE}$ ratio as a function of Y concentration.
**Fig.12.** CL spectra of pure and Y-doped ZnO sprayed films.
**Fig.13.** Variation of $I_{UV}/I_{DLE}$ ratio with Y doping.

**Table 1** Optimized parameters for the spray deposition.

| | **Optimized parameters** |
|---|---|
| Solvent | Deionized water |
| Substrate temperature | 450 ºC |
| Carrier gas | Air |
| Spray rate (ml.min$^{-1}$) | 1 |
| Zinc chloride (M) | 0.05 |
| Yttrium (at. %) | 0, 2, 5, 7 at% (Yttrium acetate hydrate) |
| Substrate | Glass |

**Table 2.a** X-ray investigation of ZnO:Y thin films.

| Sample | Position of 2**θ** (º) | Interplanar spacing | Lattice parameters | Lattice |
|---|---|---|---|---|

| | $d_{hkl}$ (Å) (±5%) | | | | compactness c/a | |
|---|---|---|---|---|---|---|
| | (100) | (200) | $d_{100}$ | $d_{200}$ | | |
| Pure ZnO | 31.77 | 34.44 | 2.814 | 2.602 | a= 3.24<br>c= 5.20 | 1.601 |
| ZnO: Y 2% | 31.61 | 34.33 | 2.828 | 2.828 | a= 3.26<br>c= 5.22 | 1.598 |
| ZnO: Y 5% | 31.61 | 34.30 | 2.828 | 2.612 | a= 3.26<br>c= 5.22 | 1.599 |
| ZnO: Y 7% | 31.80 | 34.45 | 2.811 | 2.601 | a= 3.24<br>c= 5.20 | 1.602 |

**Table 2.b** Structural parameters of pure ZnO and ZnO:Y films.

| Sample | Grain size (nm) | | Micro-strain $\varepsilon$ ($10^{-4}$) (±5.5%) |
|---|---|---|---|
| | Scherrer | FESEM | |
| Intrinsic ZnO | 48 | 116 | 13.7 |
| ZnO:Y 2% | 49 | 140 | 13.6 |
| ZnO:Y 5% | 52 | 157 | 12.7 |
| ZnO:Y 7% | 47 | 86 | 14.1 |

**Table 3** Calculated values of the optical band gap $E_g$

| | Y content Y/ZnO (%) | | | |
|---|---|---|---|---|
| | 0 | 2 | 5 | 7 |
| $E_g$(eV) | 3.12 | 3.14 | 3.18 | 3.15 |

**Table 4** Values of Urbach energy $E_u$

| Sample | $E_u$(meV |
|---|---|
| Pure ZnO | 103.90 |
| $Zn_{0.98}Y_{0.02}O$ | 100.47 |
| $Zn_{0.95}Y_{0.05}O$ | 77.14 |
| $Zn_{0.93}Y_{0.07}O$ | 93.04 |

**Table 5** The calculated values of $I_{uv}/I_{vis}$ ratio.

| Sample | ZnO:Y 0% | ZnO:Y 2% | ZnO:Y 5% | ZnO:Y 7% |
|---|---|---|---|---|
| $I_{uv}/I_{vis}$ | 2.82 | 3.16 | 10.46 | 20.71 |

.

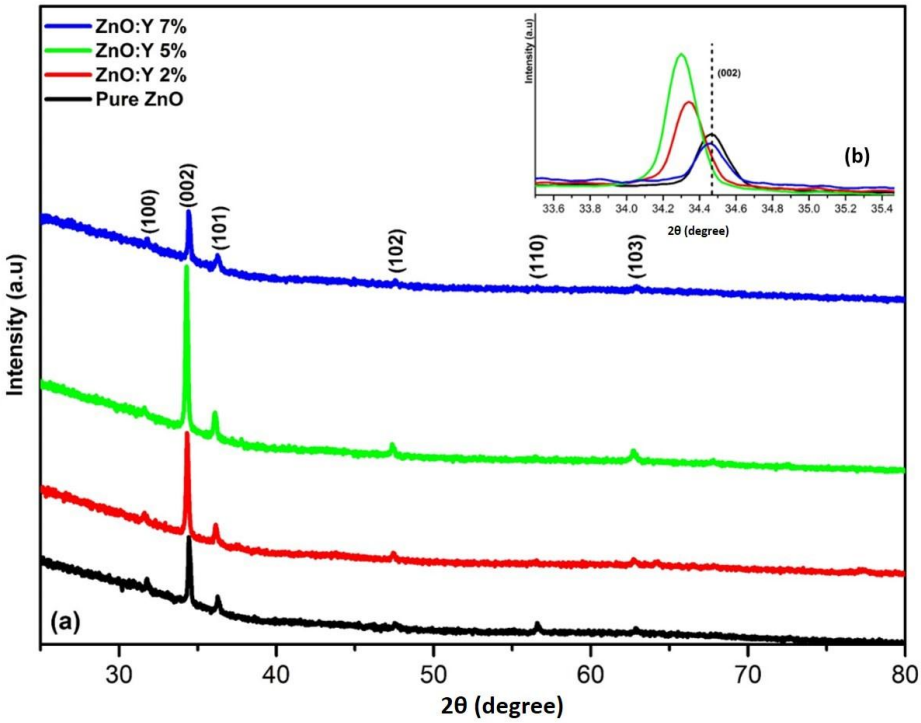

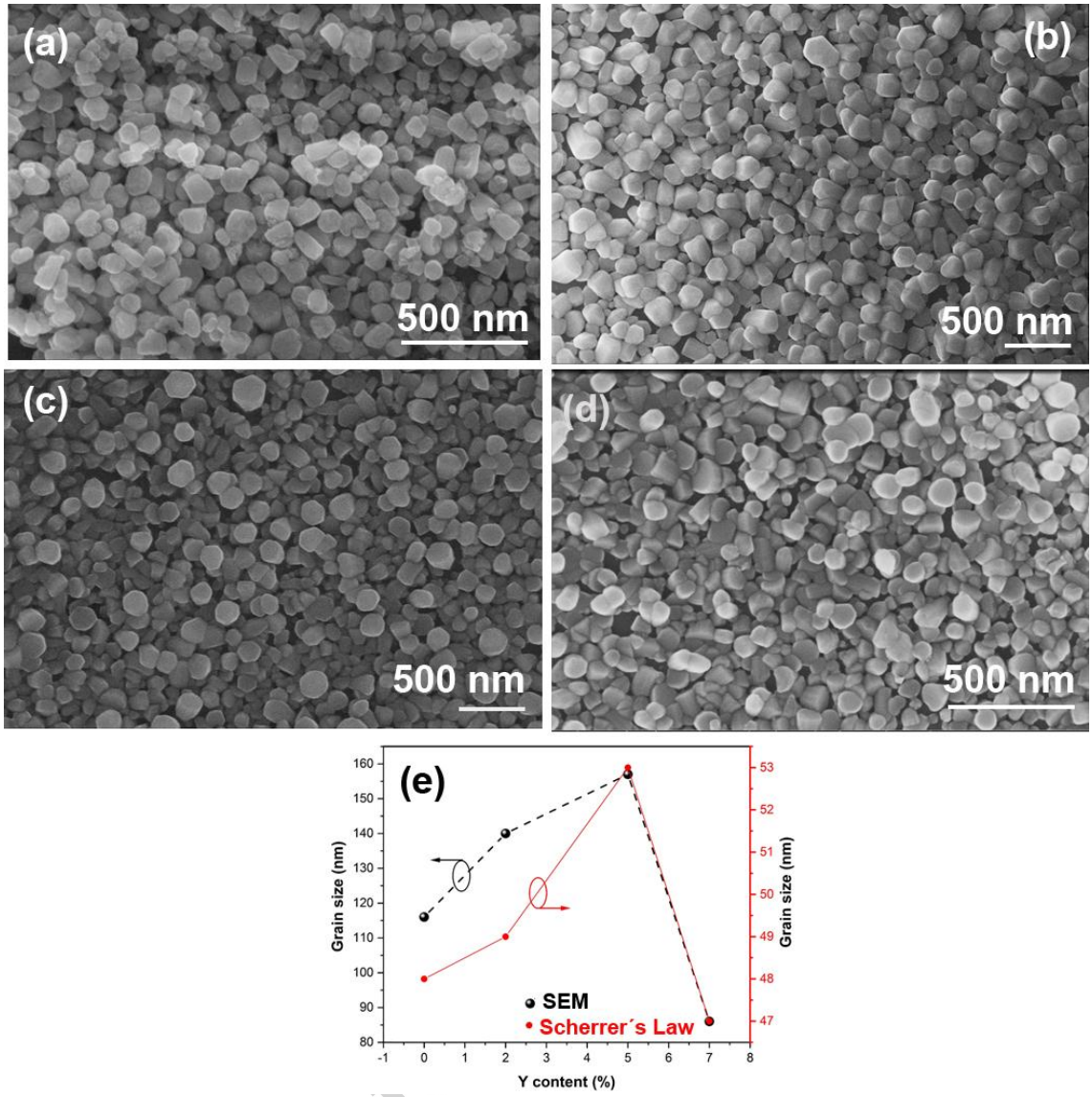
(a)
500 nm
(b)
500 nm
(c)
500 nm
(d)
500 nm
(e)
Grain size (nm)
Grain size (nm)
Y content (%)
SEM
Scherrer´s Law

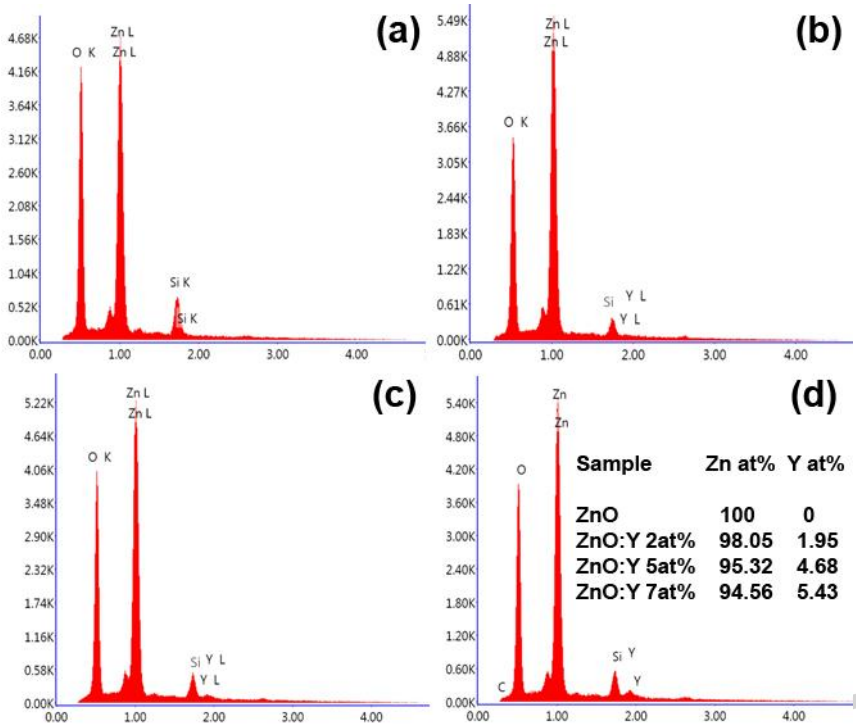

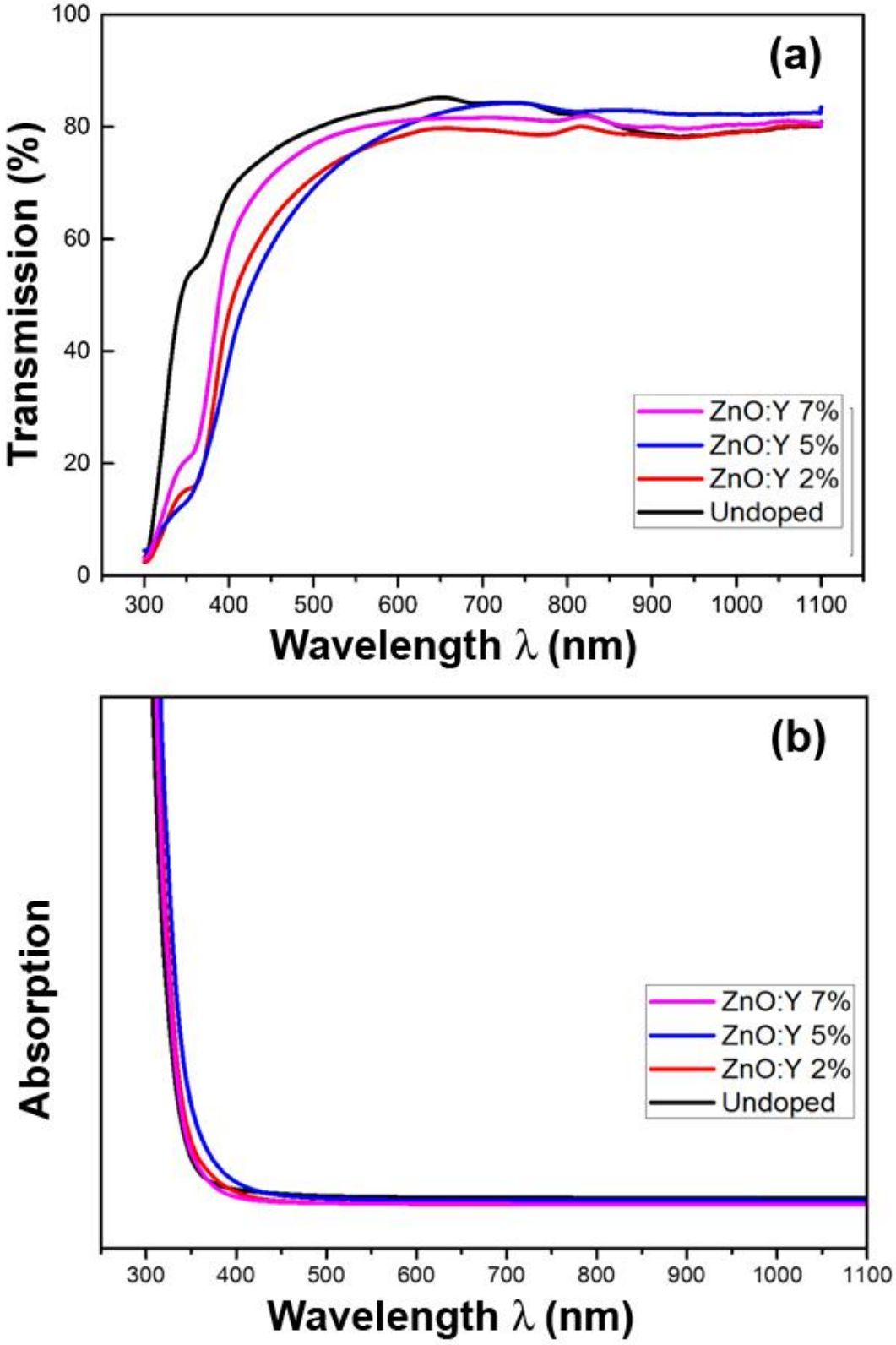
(a)
Transmission (%)
100
80
60
40
20
0
300
400
500
600
700
800
900
1000
1100
Wavelength λ (nm)
ZnO:Y 7%
ZnO:Y 5%
ZnO:Y 2%
Undoped
(b)
Absorption
300
400
500
600
700
800
900
1000
1100
Wavelength λ (nm)
ZnO:Y 7%
ZnO:Y 5%
ZnO:Y 2%
Undoped

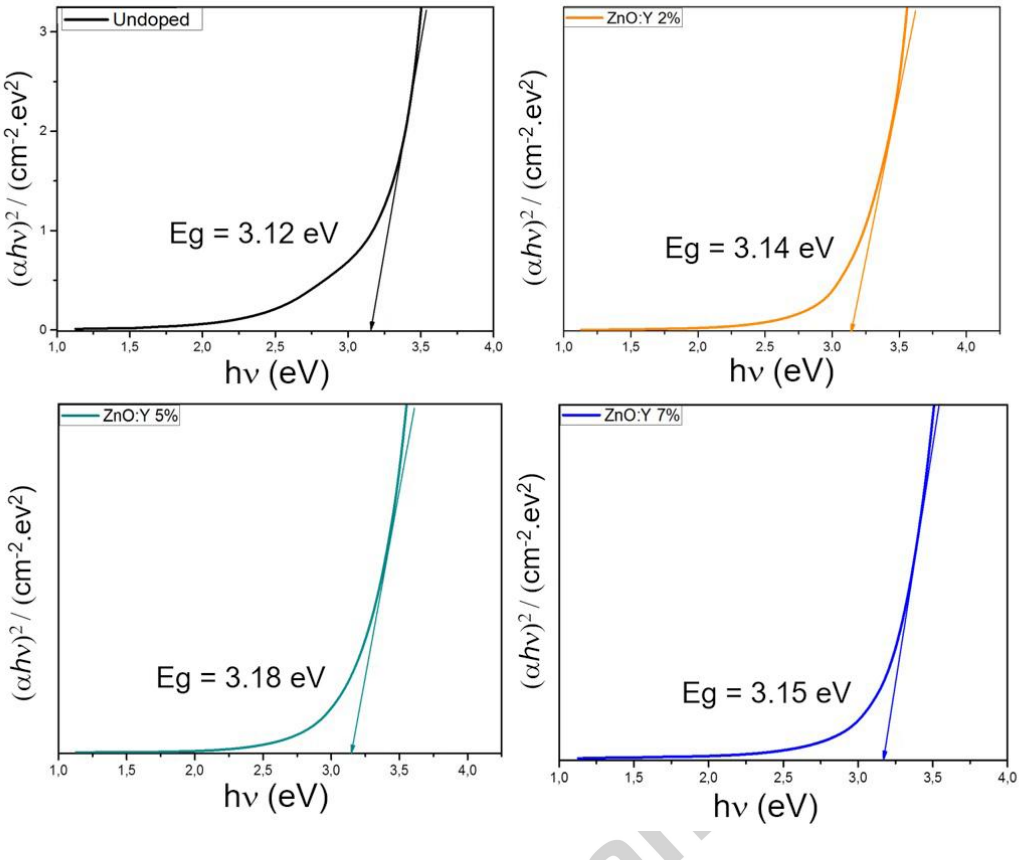
Undoped
Eg = 3.12 eV
ZnO:Y 2%
Eg = 3.14 eV
ZnO:Y 5%
Eg = 3.18 eV
ZnO:Y 7%
Eg = 3.15 eV
(αhν)² / (cm⁻².eV²)
hν (eV)

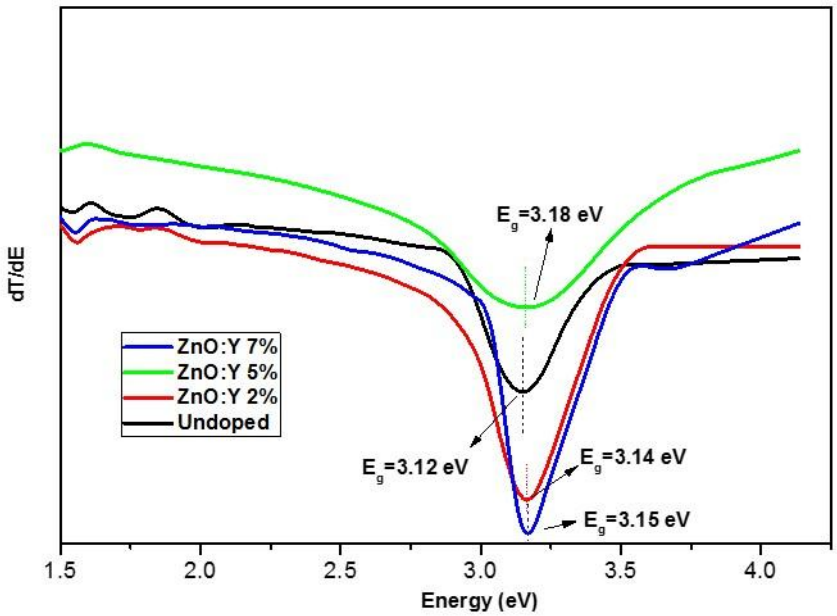
dT/dE
Energy (eV)
ZnO:Y 7%
ZnO:Y 5%
ZnO:Y 2%
Undoped
Eg=3.18 eV
Eg=3.12 eV
Eg=3.14 eV
Eg=3.15 eV

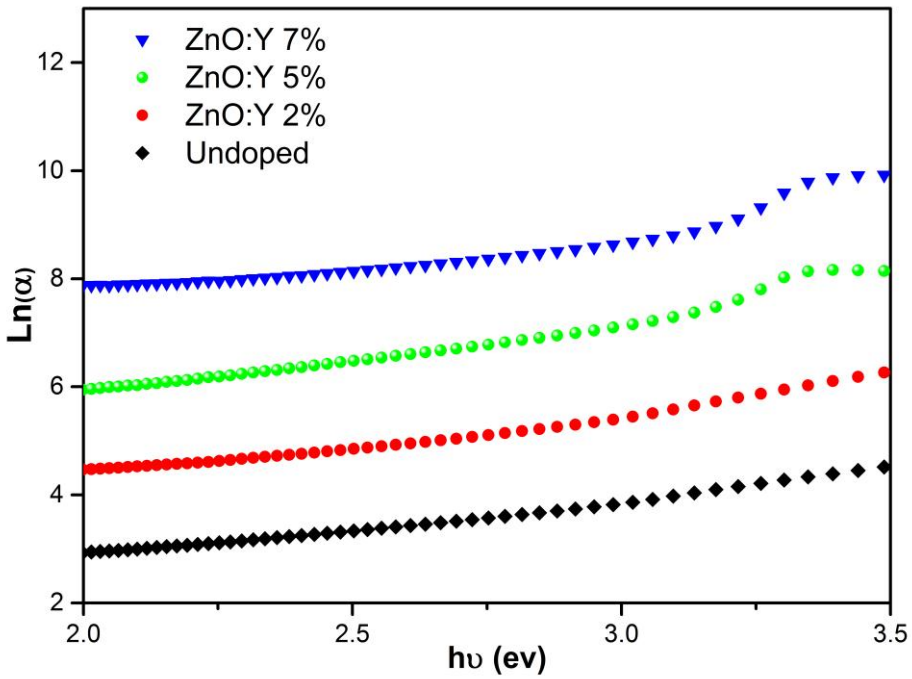
ZnO:Y 7%
ZnO:Y 5%
ZnO:Y 2%
Undoped
Ln(α)
hυ (ev)
12
10
8
6
4
2
2.0
2.5
3.0
3.5

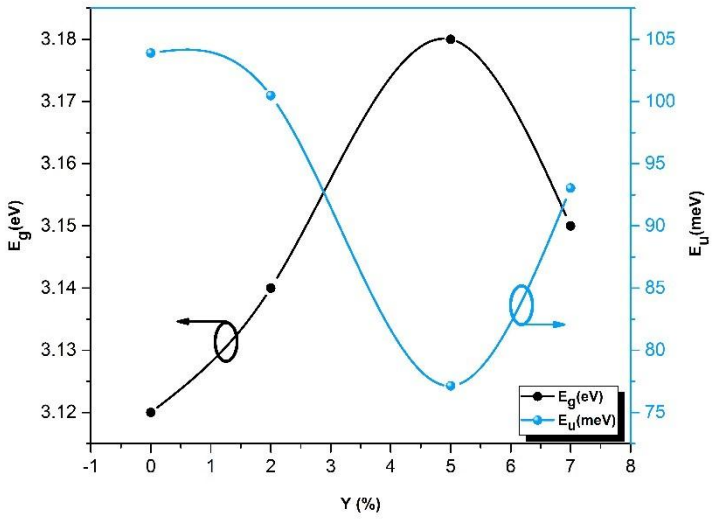
E_g(eV)
E_u(meV)
Y (%)
3.18
3.17
3.16
3.15
3.14
3.13
3.12
105
100
95
90
85
80
75
-1
0
1
2
3
4
5
6
7
8

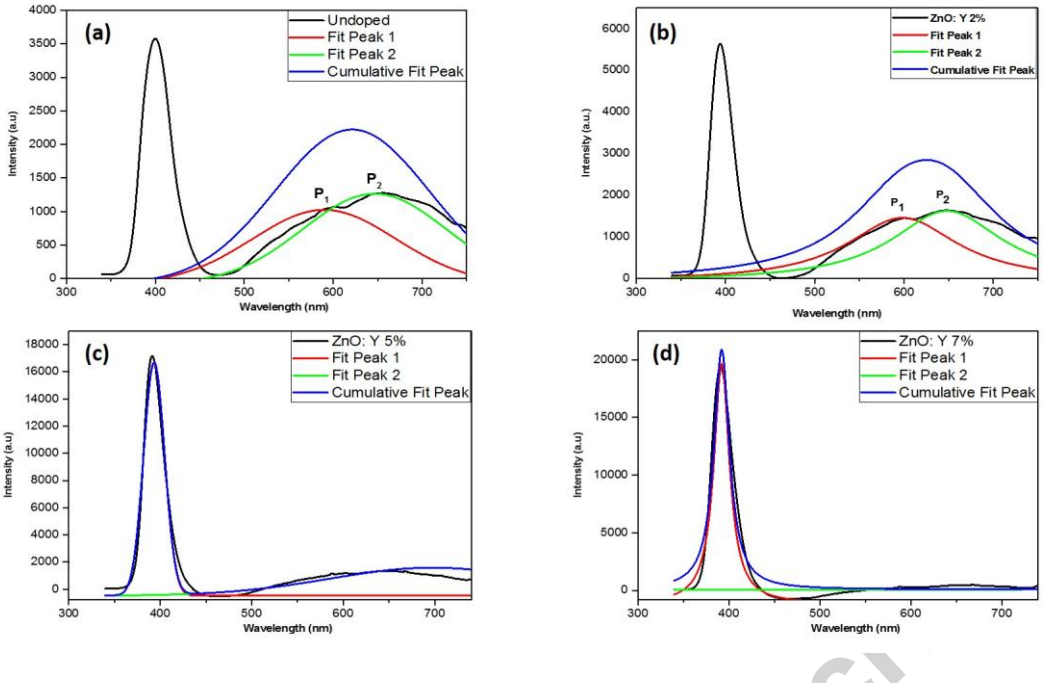
(a)
Undoped
Fit Peak 1
Fit Peak 2
Cumulative Fit Peak
P1
P2
Intensity (a.u)
Wavelength (nm)
(b)
ZnO: Y 2%
Fit Peak 1
Fit Peak 2
Cumulative Fit Peak
P1
P2
Intensity (a.u.)
Wavelength (nm)
(c)
ZnO: Y 5%
Fit Peak 1
Fit Peak 2
Cumulative Fit Peak
Intensity (a.u)
Wavelength (nm)
(d)
ZnO: Y 7%
Fit Peak 1
Fit Peak 2
Cumulative Fit Peak
Intensity (a.u)
Wavelength (nm)

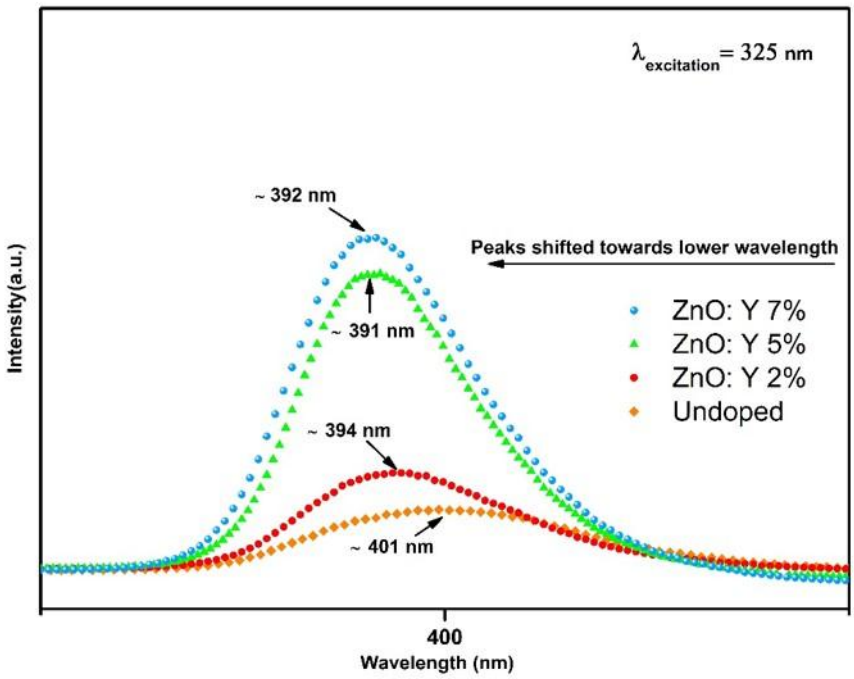
λexcitation = 325 nm
~ 392 nm
Peaks shifted towards lower wavelength
~ 391 nm
ZnO: Y 7%
ZnO: Y 5%
ZnO: Y 2%
Undoped
~ 394 nm
~ 401 nm
Intensity(a.u.)
400
Wavelength (nm)

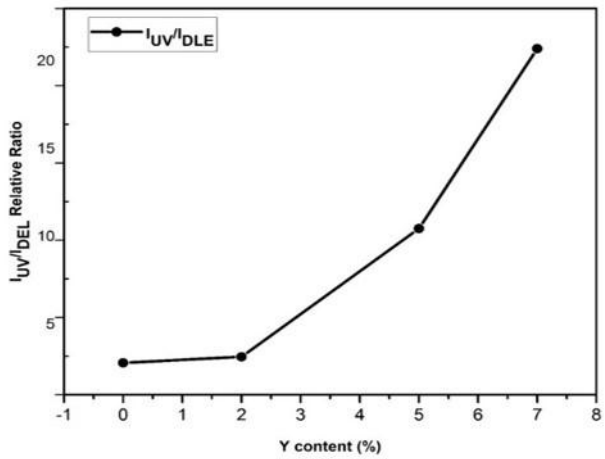
$I_{UV}/I_{DLE}$
$I_{UV}/I_{DEL}$ Relative Ratio
Y content (%)

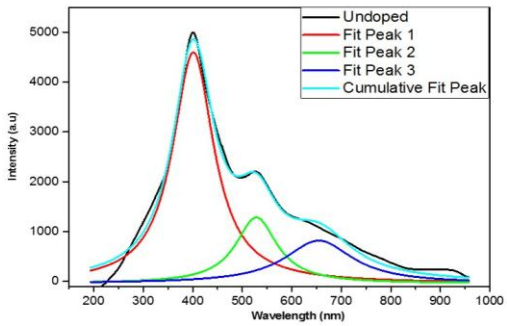
Undoped
Fit Peak 1
Fit Peak 2
Fit Peak 3
Cumulative Fit Peak
Intensity (a.u)
Wavelength (nm)

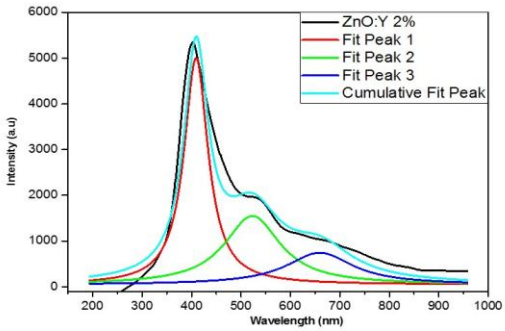
ZnO:Y 2%
Fit Peak 1
Fit Peak 2
Fit Peak 3
Cumulative Fit Peak
Intensity (a.u)
Wavelength (nm)

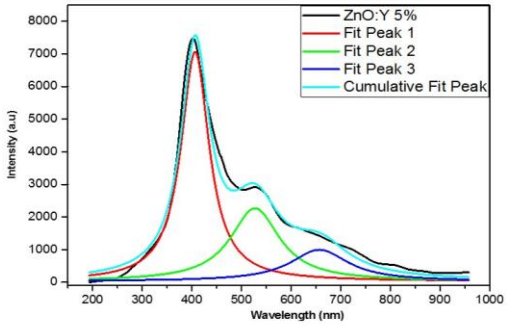
ZnO:Y 5%
Fit Peak 1
Fit Peak 2
Fit Peak 3
Cumulative Fit Peak
Intensity (a.u)
Wavelength (nm)

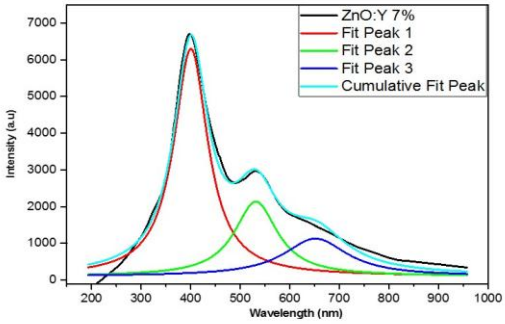
ZnO:Y 7%
Fit Peak 1
Fit Peak 2
Fit Peak 3
Cumulative Fit Peak
Intensity (a.u)
Wavelength (nm)